IJPSR (2016), Vol. 7, Issue 2 **(Research Article)**

INTERNATIONAL JOURNAL OF PHARMACEUTICAL SCIENCES AND RESEARCH

Received on 07 August, 2015; received in revised form, 24 September, 2015; accepted, 05 December, 2015; published 01 February, 2016

3D-QSAR AND CONTOUR MAP ANALYSIS OF TARIQUIDAR ANALOGUES AS MULTIDRUG RESISTANCE PROTEIN-1 (MRP1) INHIBITORS

Prathusha Kakarla [1], Madhuri Inupakutika [2], Amith R. Devireddy [2], Shravan Kumar Gunda [3], Thomas Mark Willmon [1], Ranjana KC [1], Ugina Shrestha [1], Indrika Ranaweera [1], Alberto J. Hernandez [1], Sharla Barr [1], And Manuel F. Varela*[1]

Department of Biology [1], Eastern New Mexico University, Station 33, Portales, NM, 88130, USA.
Department of Biological Sciences [2], College of Arts and Sciences, University of North Texas, 1155 Union Circle #305220, Denton, TX 76203, USA.
Bioinformatics Division [3], Osmania University, Hyderabad-500007, Andhra Pradesh, India.

Keywords:

QSAR, CoMFA, CoMSIA, Anti-cancer therapy, MDR, MRP1, Tariquidar, Contour map analysis, Efflux, Modulation, Inhibition, Cancer, ABC transporters

Correspondence to Author:
Manuel F. Varela

Professor of Biology,
Department of Biology, Eastern New Mexico University, 1500 S Ave K, Station 33, Portales, NM, 88130, USA.

Email: manuel.varela@enmu.edu

ABSTRACT: One of the major obstacles to the successful chemotherapy towards several cancers is multidrug resistance of human cancer cells to anti-cancer drugs. An important contributor to multidrug resistance is the human multidrug resistance protein-1 transporter (MRP1), which is an efflux pump of the ABC (ATP binding cassette) superfamily. Thus, highly efficacious, third generation MRP1 inhibitors, like tariquidar analogues, are promising inhibitors of multidrug resistance and are under clinical trials. To maximize the efficacy of MRP1 inhibitors and to reduce systemic toxicity, it is important to limit the exposure of MRP1 inhibitors and anticancer drugs to normal tissues and to increase their co-localization with tumor cells. Comparative Molecular Field Analysis (CoMFA) and Comparative Molecular Similarity Indices Analysis (CoMSIA) associated with 3D-Quantitiative structure-activity relationship (3D-QSAR) studies were performed on a series of tariquidar analogues, as selective MDR modulators. Best predictability was obtained with CoMFA model r^2(non-cross-validated square of correlation coefficient) = 0.968, F value = 151.768 with five components, standard error of estimate = 0.107 while the CoMSIA yielded r^2 = 0.982, F value = 60.628 with six components, and standard error of estimate = 0.154. These results indicate that steric, electrostatic, hydrophobic (lipophilic), and hydrogen bond donor substituents play significant roles in multidrug resistance modulation of tariquidar analogues upon MRP1. The tariquidar analogue and MRP1 binding and stability data generated from CoMFA and CoMSIA based 3D-contour maps may further aid in study and design of tariquidar analogues as novel, potent and selective MDR modulator drug candidates.

INTRODUCTION: Multidrug resistance and ABC transporters: Multidrug resistance in cancer can significantly hamper the response to chemotherapy and increase the likelihood of mortality [1, 2].

QUICK RESPONSE CODE

DOI: 10.13040/IJPSR.0975-8232.7(2).554-72

Article can be accessed online on: www.ijpsr.com

DOI link: http://dx.doi.org/10.13040/IJPSR.0975-8232.7 (2).554-72

Multidrug resistance occurs when cancer cells exposed to one anticancer drug show cross-resistance to various anticancer drugs that are structurally and functionally different [1]. Intrinsic and acquired MDR has long been recognized as causes of chemotherapeutic failure [3]. Acquired multidrug resistance is highly problematic in cases where drugs respond to chemotherapy in the beginning but lose sensitivity later [4]. Over expression within the cellular membrane of different efflux pumps from various transporter families can lead to multidrug resistance [5].

Expression of primary active (energy-dependent) ATP-binding cassette (ABC) efflux pumps has been linked to tumor aggressiveness in different tumor types as the drugs are carefully channeled across the biological membrane [1]. ABC transporters are highly expressed in pharmacologically important tissues and translocate a wide variety of solutes across biological membranes [1]. Thus, efflux by ABC transporters serves to detoxify and protect cells from anticancer compounds and have been found to be critical in the absorption, excretion, and distribution of drugs [6]. Elevated expression of ABC transporters and insertion into the bacterial cell membrane decrease the bioavailability of drugs by hindering cellular accumulation below the required standard threshold or by redistributing anticancer drugs away from target organelles, thus conferring MDR (**Fig. 1**) [6]. Therefore, ABC transporters are important elements which should be considered when developing anti-cancer drugs; especially when developing specifically targeted MDR-cancer therapy [7].

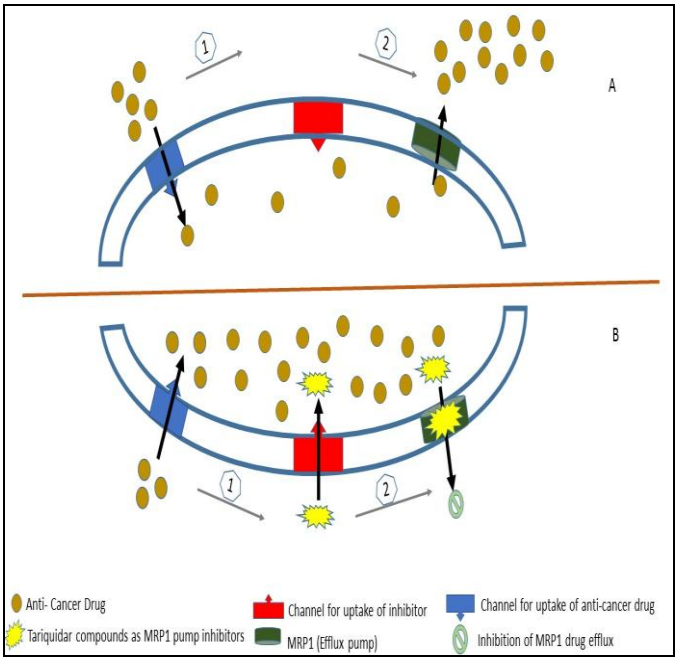

FIG.1: MRP1 EFFLUX AND TARIQUIDAR ANALOGUES AS MRP1 EFFLUX BLOCKERS

Fig. 1 A illustrates the efflux mechanism MRP1 employs to pump anti-cancer drugs out of the cell, thereby imparting drug resistance to cancer cells. In step 1, anti-cancer drug enters the cancer cell through porins. In this case, there is no MRP1 inhibitor in the extracellular space to be taken up by the cancer cell porins. In step 2, because of the absence of MRP1 inhibitor, the efflux mechanism by MRP1 is activated, pumping the anti-cancer drug out of the cancer cell. This leads to decreased concentrations of anti-cancer drug inside the cell, and thus the cancer cell resists the drug and survives. **Fig. 1 B** illustrates the MRP1 efflux blocking mechanism. In step 1, anti-cancer drug enters the cancer cell through porins. There are tariquidar analogues present in the extracellular space of the cancer cell. These tariquidar analogues will be taken up by the cancer cell through porins. These tariquidar analogues will block the MRP1 efflux pump. In step 2, as the MRP1 efflux pump is blocked, anti-cancer drugs will stay in the cancer cell. Increased concentration of anti-cancer drug inside the cancer cell will aid in the death of the cancer cell. MRP1 blockers can effectively inhibit anti-cancer drug efflux thereby enhancing the efficacy of anti-cancer therapy [8].

Multidrug resistance protein 1 (MRP1):

Of the fifty different human ABC transporters from seven subfamilies, over-expressed P-glycoprotein (P-gp), multidrug resistance protein 1 (MRP1)/ABCC1, and breast cancer resistance protein (BCRP)/ABCG2/MXR/ABCP were found to be critical for dissemination of multidrug resistance in cancer cells [9]. MRP1 (NCBI ID: NP_004987) (www.ncbi.nlm.nih.gov/protein) (Uni Prot ID: P33527) (www.uniprot.org) located on chromosome 16p13.1 is a 190 kDa (1531 amino acids) efflux pump encoded by the human genes *ABCB1* and *ABCC1* which confer multidrug resistance [10, 11]. MRP1 extrudes anti-cancer drug as substrates, allowing the growth of cancers, including those of the lung, breast and prostate, as well as of childhood neuroblastoma [12].

The structure of the MRP1 pump contains 17 transmembrane (TM) helices distributed between three TM membrane spanning domains (MSD) for substrate recognition and transport and two cytosolic nucleotide-binding domains (NBD) for energy generation by ATP hydrolysis **(Fig. 2)** [3, 13, 14]. The two NBDs form a common binding site where the energy of ATP is harvested to promote drug efflux through a pore that is delineated by the TM helices [15-17]. Comparing the sequences of various ABC proteins, Nucleotide binding sites

revealed the presence of conserved signature sequence motifs in NBD1 and NBD2 namely, Walker A, Walker B, Motif C, Q loop, D loop, and H loop [18]. The Q, D and H loops contain highly conserved Glu, Asp, and His residues, respectively, contributing to stabilization and catalysis on binding of nucleotides. In NBD1, the conserved sequence of Walker A is GXXGXGKS; Q- loop is QXXWIXN; C motif is LSGGQXXR; Walker B is XYI/LXD; D loop is SAV/LD; and H-loop is TXX. In NDB2, the conserved sequence of Walker A is GXXGXGKS; Q- Loop is DDXXXXXG; C motif is LSXGXRQ; Walker B is I/VI/LXXD; D-Loop is XAXD; and H-loop is XHR [18]. On binding, conformational changes in Walker A and Q loop were predicted according to the hypothetical MRP1 transport model (**Fig.2**) [19-21].

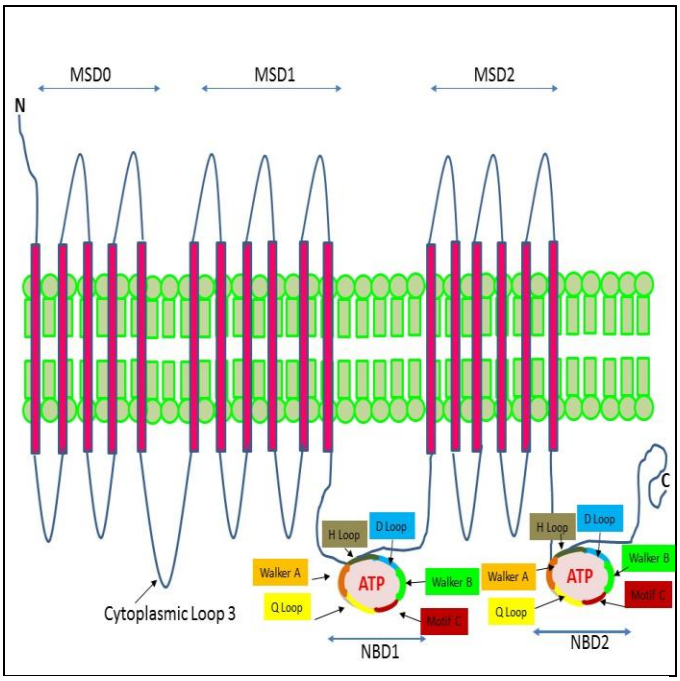

FIG. 2: TWO-DIMENSIONAL (2D) STRUCTURE OF MULTIDRUG RESISTANCE PROTEIN 1 (MRP1)

This Fig. indicates 17 transmembrane domains distributed between membrane spanning domains (MSD) 0, 1 and 2. MSD0 and MSD1 are connected together by a cytoplasmic loop 3 (CL3). MSD1 is connected to MSD2 by a nucleotide binding domain (NBD), hosting an ATP binding site with conserved signature sequences. MSD2 is connected to the C- terminal by an NBD2 domain. In NBD1, and NMD2, various conserved sequences are represented in colors. Signature sequence for Walker A is GXXGXGKS; Q- loop is QXXWIXN; C motif is LSGGQXXR; Walker B is XYI/LXD; D loop is SAV/LD; and H-loop is TXX. In NDB2, the conserved sequence of Walker A is GXXGXGKS; Q- Loop is DDXXXXXG; C motif is LSXGXRQ; Walker B is I/VI/LXXD; D-Loop is XAXD; and H-loop is XHR [18, 20].

The MRP1 transporter is expressed in intestine, liver, and kidney cells as well as in the blood brain barrier and regulates the intracellular concentrations of substances by transporting a broad variety of organic anions out of the cell [22, 23]. The MRP1 transporter and glutathione conjugates play pivotal roles in mediating drug resistance by modulating pharmacokinetics and altering the bioavailability and toxicity of anticancer compounds, such as anthracyclines, epipodophyllotoxins, vinca alkaloids, camptothecins, vincristine, daunorubicin, taxanes, topoisomerase inhibitors, and antimetabolites [24-26].

Tariquidar analogues to block MRP1 efflux:

Blocking of these MRP1 transporters, which represent significant barriers to chemotherapy, can aid in effective reversal of multidrug resistance in cancer patients [26]. One strategy for the reversal of MRP1transporter-associated chemo-resistance is the combined use of anticancer drugs with efflux modulators or inhibitors that act as chemo sensitizers [26]. Specific binding at the MRP1 active site on cancer cells and related clinical toxicity of currently available MRP1 modulators is uncertain; exploring novel and potent non-toxic modulators with high specificity for cancer cell embedded MRP1 active site is critical [27]. Tariquidar (XR9576) is a MRP1 inhibitor undergoing investigation as an adjuvant against multidrug resistance in cancer (**Fig.3**) [8].

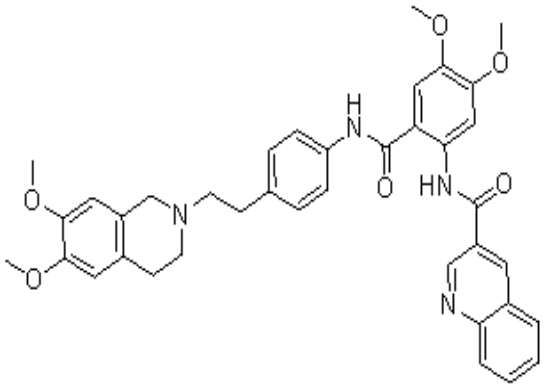

FIG. 3: CHEMICAL STRUCTURE OF TARIQUIDAR (XR9576) DRAWN USING ISIS. (Adopted from[8])

Tariquidar non-competitively binds to the MRP1 transporter, thereby inhibiting efflux of anticancer drugs across the membrane showing significant effects on the pharmacokinetics of paclitaxel, doxorubicin, and vincristine **(Fig.1)**[8, 28]. Previous studies have shown that tariquidar analogues act like MRP1 modulators, thus possibly enhancing the therapeutic potential of anticancer drugs by blocking efflux pumps and overcoming multidrug resistance [8, 29]. Inhibition of drug transport across the membrane may result in increased intracellular concentrations of an anticancer drug, thereby augmenting its cytotoxicity [30, 31].

The mechanism of tariquidar analogues acting as MRP1 efflux blockers is delineated in **Fig.1** [29, 32-34]. Because these compounds demonstrate high activity at clinically achievable concentrations, we anticipate that this class of drugs will be a promising and valuable tool for future applications in the fight against cancer and drug resistance [28, 34-37].

Molecular modeling, docking, 3D- QSAR and contour map analysis:

Molecular modeling attempts to be the perfect algorithm for fitting flexible molecules into the active sites of corresponding selected proteins [38]. FlexX exploits molecular flexibility of the ligand, and the development of a docking model includes the physicochemical properties of the molecules [39]. Using FlexX to "dock" potential drugs gives important insights into their binding mechanisms and makes a focused optimization of the potential drug molecule possible [40].

3D QSAR analyses generate virtual receptors and determine the quantitative relationships between the biological activity of a set of compounds and their 3D properties via statistical correlation methods [41]. The basic principle behind CoMFA is that changes in binding affinities of ligands are related to changes in shape and strength of non-covalent interaction fields surrounding the molecules, such as steric, electrostatic, hydrophobic, and hydrogen bond accepting or donating fields [42, 43]. The CoMFA QSAR equation is summarized graphically as a 3D contour map, showing those fields in which the lattice points are associated with extreme values [44, 45]. These contour map values correspond to the molecular fields which are considered crucial for binding affinity[44, 46]. CoMSIA is an extension of the CoMFA and involves comparison of molecular similarity, given in terms of similarity indices [47]. In CoMSIA, steric and electrostatic fields along with hydrophobic fields and hydrogen bond donor/acceptor fields are computed [47].

Computational methods:

Molecular modeling:

Homology modeling was adopted in order to construct a three dimensional (3D) structure for human MRP1 protein (NCBI ID: NP_004987). This protein was further employed to perform docking and contour map studies. Swiss-model was employed to thread all the possible templates and to construct the best homology model of MRP1 protein. The crystal structure of the multidrug transporter P-glycoprotein (PDB code: 4F4C; www.pdb.org) was used as a base template to construct the 3D model for MRP1. The quality of the model was analyzed using QMEAN4 (Qualitative Model Energy Analysis 4) and GMQE (Global Model Quality Estimation**)** values generated by the Swiss-model server.

Geometry optimization:

Twenty six tariquidar analogues reported to be efficient MRP1 blockers were chosen for this study [8]. IC_{50} values available in the literature were used to calculate pIC_{50} (-log IC_{50}) values for all of the 26 compounds [8]. Among those 26 tariquidar analogues, compound 18 has the least activity (pIC_{50}= 5.309804) and compound 20 (pIC_{50}= 7.420216) is highly active. Chemical structures of these 26 tariquidar analogues were drawn using ISIS, and were geometrically optimized on SYBYL using default parameters and convergence criterion of 0.001 kcal/mol (Supplementary table 1) [48]. The energy minimization of these 26 compounds was performed viatripos force field and the Gasteiger-Huckel charges using a distance-dependent dielectric and powell conjugate gradient algorithm with a convergence criterion of 0.05 kcal/mol [49, 50]. Further geometric optimization of these tariquidar analogues was done using the default set semi-empirical program MOPAC 6.0; MOPAC charges were used for entire calculations [51].

Alignment: In 3D-QSAR studies, a geometric similarity should exist between the structures, so MOPAC geometry optimized structures were aligned on the most active molecule (determined from the literature) from the set as a template[52]. Doing so adjusts the geometry of the molecules such that the steric and electrostatic fields of the molecules match the fields of the template molecule [52, 53].

Molecular docking:

Receptor-ligand docking is highly specific and is crucial for many biological functions [54]. In this study FlexX interfaced with SYBYL 6.0 was used to dock tariquidar compounds to the active site of MRP1 efflux pump protein [55]. In SYBYL 6.0 docking model, tariquidar compounds are considered to be the flexible molecules whereas MRP1 protein is predicted to be rigid. In docking automated process, all the new fragments are joined to the base fragment at the active site in every possible angle and conformation[56]. SYBYL 6.0 interfaced with FlexX was used to compute the predictable binding conformations of these 26 inhibitors around an active radius of 6.5Å17[38]. Default FlexX docking parameters were employed to obtain the docking scores. The interactions of 26 tariquidar analogues with MRP1 protein were calculated and the highest scoring compound was considered as the best fit. Energy calculations and structural information was also computed on SYBYL-FlexX.

3D- QSAR- CoMFA and CoMSIA and contour analyses:

Three-dimensional quantitative structure activity relationship (QSAR) studies that include comparative molecular field analysis (CoMFA) and molecular similarity indices in comparative analysis (CoMSIA) methods were conducted on these 26 tariquidar analogues to assess their potential as MRP1 blockers. CoMFA employs tripos force field with a distance-dependent, dielectric constant in all interactions in a regularly spaced (2×10^{-10} m) grid taking a sp3 carbon atom as steric probe and a +1 charge as electrostatic probe[38, 57]. The cut-off was set to 30 Kcal/mol [38, 57]. CoMSIA uses a Gaussian-type distance-dependent dielectric constant to minimize changes in atomic positions and charge potentials at the grids [58]. CoMSIA calculates using a C+ probe atom with a radius of 1×10^{-10} m placed at a regular grid spacing of 2×10^{-10} m to enclose all the binding conformations of the inhibitors [59]. Using default parameters, steric, electrostatic, and hydrophobic field parameters were calculated. The steric filed contribution is denoted by the third power of the atomic radii of the atoms and electrostatic properties were given as atomic charges that were obtained from FlexX docking [60].

Hydrophobicity was calculated as atom dependent parameter and an approximately 4Å lattice grid was used to include all the binding conformations of the inhibitors. In this study, similarity indices were computed using a probe atom (*W*probe,*k*) with charge +1, radius 1Å, hydrophobicity +1, and attenuation factor, a, of 0.3 for the Gaussian type distance [38]. The statistical analysis for the CoMSIA analyses was similar to CoMFA[61].

The pIC_{50} data will couple 3-log units offering a wide and similar set of data for 3D-QSAR analysis. Compounds were divided into test and training sets in 1:3 ratio to improve the predictability of the 3D-QSAR models. Cross-validation and partial least score (PLS) analyses were used where the cross-validated coefficient (q^2), leaving optimal number of components and lowest standard error of prediction, was considered for the accuracy determination of the predicted models [43, 61].

The reliability of a 3D-QSAR model depends on the activity prediction ability of the model. Pearson's correlation coefficient, r^2, is the squared correlation coefficient that measures the precision of adjustment for the fitted values to the observed ones [61]. In cross-validation, the outcome of the LOO procedure is a cross-validated correlation coefficient (r^2, cv or q^2) that indicates the robustness and predictive ability of the model [56]. The cross-validated correlation coefficient, q^2, is regarded as a measure of internal consistency of the derived model [56]. Fischer statistic (F value) parameter was used as a measure of the level of statistical significance of the regression model; a higher F value implies a more significant correlation [56].

RESULTS AND DISCUSSION:

Homology modeled protein indicating an effective 3D structural conformation: The 3D structural conformation of the molecular modeled MRP1 protein that was generated using Swiss-model server is shown in **Fig. 4**. This model was validated based on the statistically significant QMEAN4 value, indicating the current model to be close to the Z-score of the template (PDB ID: 4F4C) from PDB. A higher GMQE value close to 0.5 indicates the greater reliability of the model.

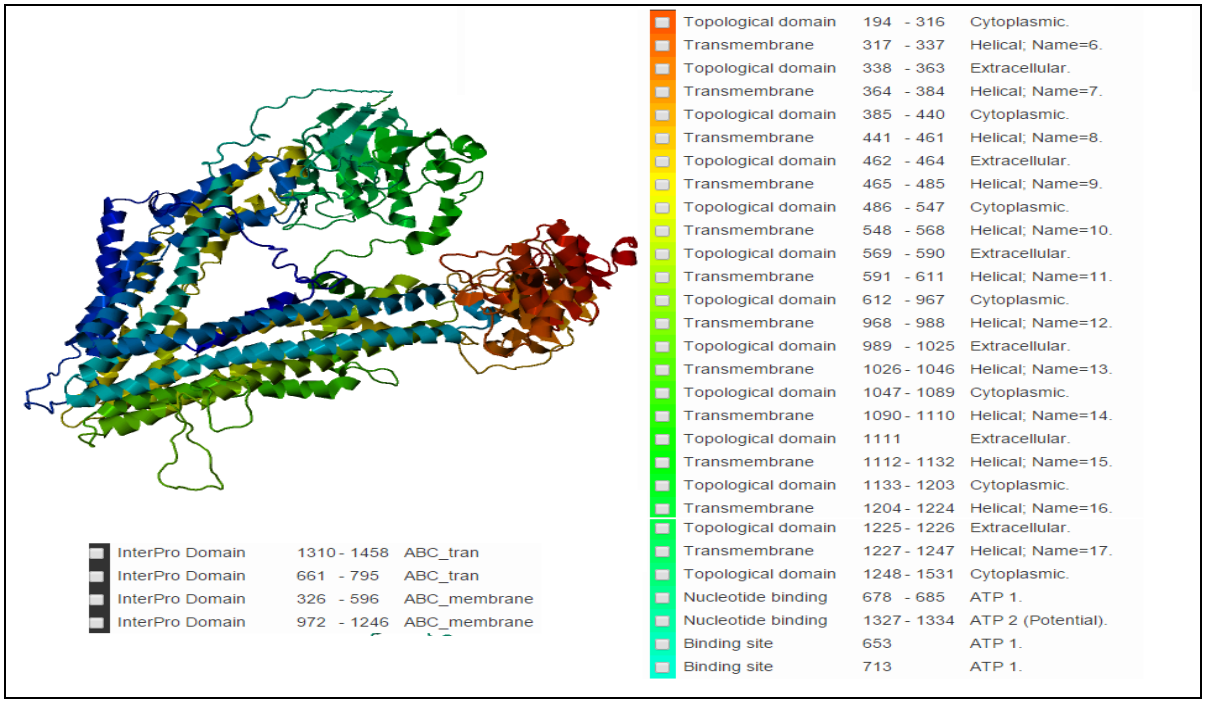

FIG. 4: FIG. 4: HOMOLOGY MODELED 3D STRUCTURAL CONFORMATION OF MRP1:
Protein structure indicating 17 TM's as helices and loops. The structure was constructed using Swiss-model (swissmodel.expasy.org) [11] and visualized on PSI (http://www.proteinmodelportal.org/).

Docking results indicate tariquidar analogues as potential MRP1 modulators because of their interaction with the MRP1 at the active site: The FlexX dock score and amino acid interactions are considered as the base with which to assess the potential of the tariquidar analogues in blocking the active site of the MRP1 drug efflux pump [11]. This docking study on tariquidar analogues as MRP1 efflux blockers predicted a considerable correlation in the FlexX scores attained. Many polar amino acid residues present in the active site of MRP1 were found to be interacting with the tariquidar analogues in this study (**Table 1**).

TABLE 1: FLEXX DOCK SCORES; INTERACTING AMINO ACIDS, MOLECULES AND ATOMS OF TARIQUIDAR ANALOGUE COMPOUNDS THAT ARE SIGNIFICANT FOR BINDING TO THE MRP1 ACTIVE SITE AND THEIR DISTANCES FROM MRP1 PROTEIN.

S. No	Interacting amino acids, molecules or atoms	FlexX dock score	Distance (Å)	No. of interactions
1	GLN 713	-15.0	2.08	
	O3		2.20	
	LYS 684		2.12	5
			2.26	
	GLY 681		1.67	
2	O3	-14.8	2.23	
	GLN 713		2.11	
	GLY 681		1.65	6
	LYS 684		1.69	
			2.15	
			2.28	

3	GLN 713	-14.8	2.11	
	O3		2.23	
	LYS 684		1.69	6
			2.28	
			2.15	
	GLY 618		1.65	
4	LYS 684	-15.2	2.06	
			2.26	
			1.77	
	GLY 681		1.90	7
	O3		2.53	
			3.41	
	GLN 713		2.04	
5	GLN 713	-20.7	2.04	
	LYS 684		1.92	
	VAL 680		1.78	5
	GLY 681		2.36	
			1.88	
6	GLN 713	-19.1	1.97	
	LYS 684		1.91	
	VAL 680		1.89	5
	GLY 681		2.37	
			1.83	
7	GLY 681	-22.4	2.05	
			2.28	
	VAL 680		1.89	5
	LYS 684		2.10	
	GLN 713		2.02	
8	ASN94	-26.5	2.75	
			1.39	
	O3		2.34	
			2.33	
	SER 686		2.40	
	GLY 683		1.93	10
			1.72	
	LYS 684		2.17	
			2.44	
	GLY 681		2.24	
9	GLN 713	-31.4	2.01	
	Mg2+		1.79	
	LYS 684		1.94	
			1.99	
			1.99	
	GLY 683		2.07	
	GLN 713		2.01	
	03		2.19	14
			2.57	
			1.68	
	SER 686		4.97	
			2.68	
			2.15	
	ASN94		2.76	

10	GLY 681	-26.6	2.18	
	LYS 684		1.69	
			2.68	
	SER 685		2.15	
			2.64	
			2.66	
	Mg2+		2.12	
			1.82	
	GLN 713		1.73	
			2.04	17
			2.39	
	O3		2.93	
			2.26	
			2.93	
			2.68	
			2.39	
			0.93	
11	SER 685	-18.9	2.65	
	SER 686		2.18	
	GLY 683		1.76	
	LYS 684		2.16	6
	O3		1.77	
			0.78	
12	GLY 681	-24.9	1.56	
			1.76	
			2.20	
	VAL 680		2.04	6
	GLN 713		2.05	
	LYS 684		1.90	
13	LYS 684	-24.9	1.90	
	GLN 713		2.05	
	GLY 681		2.20	
			1.56	6
			1.76	
	VAL 680		2.04	
14	GLN 713	-22.0	2.11	
	LYS 684		2.09	
	VAL 680		1.89	
			2.31	6
	GLY 681		1.92	
			1.60	
15	GLY 681	-26.8	1.85	
			2.10	
	VAL 680		1.80	
			2.31	6
	LYS 684		1.98	
	GLN 713		2.05	
16	GLN 713	-22.2	2.22	
	GLY 681		1.84	
			1.74	5
	THR 660		2.11	
			1.59	
17	O3	-22.1	2.10	

	ASN94		2.60	
	GLY 683		2.0	
	LYS 684		1.93	6
			2.32	
	GLY 681		1.94	
18	GLN 713	-24.6	2.08	
	VAL 680		1.99	
	GLY 681		2.29	
	LYS 684		2.00	6
	LYS 682		2.02	
			1.66	
19	LYS 684	-21.7	2.09	
	VAL 680		1.89	
	GLY 681		1.92	
			2.31	6
			1.60	
	GLN 713		2.11	
20	GLN 713	-23.2	4.78	
			2.11	
	O3		2.48	
	SER 686		2.06	
	ASN94		2.81	
			2.46	
	GLY 681		1.90	11
	LYS 684		2.06	
			2.26	
			5.00	
			1.76	
21	GLY 681	-20.7	1.64	
			2.21	
	VAL 680		1.94	4
	GLN 713		1.87	
22	GLY 681	-21.2	2.40	
			1.83	
	VAL 680		1.97	5
	LYS 684		1.98	
	GLN 713		2.06	
23	GLN 713	-21.5	1.74	
	LYS 684		1.89	
	VAL 680		2.12	
			2.06	
	GLY681		2.08	6
			1.78	
24	GLN 713	-24.2	1.76	
	O3		1.76	
			2.44	
			1.53	
			1.33	
	ASN94		2.10	
	SER 686		1.79	
			2.42	13
			2.89	
			2.66	

	LYS 684		1.99	
			2.32	
	GLY 683		2.11	
25	TRP 633	-30.3	2.190	
	SER 686		1.807	
			1.725	
	SER 685		1.792	
			2.554	
	LYS 684		2.206	11
			2.143	
			2.367	
			2.610	
	LYS 682		2.687	
	GLY 681		2.674	
26	GLN 713	-19.6	1.93	
	GLY 681		1.70	
			2.16	5
	VAL 680		2.03	
			1.89	

The FlexX dock scores and the interactions of all 26 tariquidar analogues with the active site of MRP1 are tabulated in **Table 1**. Among the 26 compounds docked, compound 9 showed 14 interactions with the active site of MRP1 and has a highest dock score of -31.4 KJ/mol (**Fig. 5)** Compound 2 has shown the lowest dock score of -14.8 KJ/ mol with six interactions (**Fig. 8**). Compound 20, most active compound, has shown a significant dock score of -23.2 KJ/mol with 11 interactions (**Fig.6**) and Compound 18, the least active compound, has shown a dock score of -24.6 KJ/ mol with six interactions with the active site of MRP1 protein (**Fig. 7**).

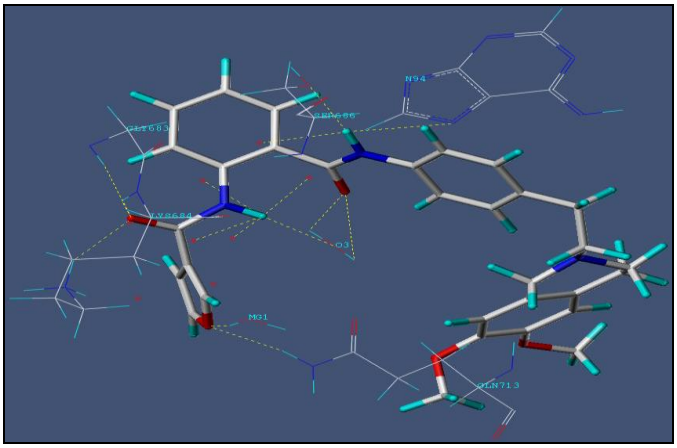

FIG. 5: COMPOUND 9 SHOWING 14 INTERACTIONS (REPRESENTED AS YELLOW LINES) WITH THE ACTIVE SITE OF MRP1 AND HAVING THE HIGHEST DOCK SCORE OF -31.4 KJ/MOL.

The structure in ball-and-stick model represents compound 9, and the structure in lines represents MRP1 protein.

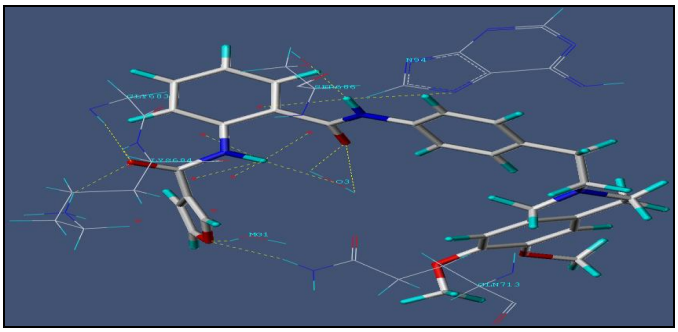

FIG.6: FIGURE SHOWING INTERACTIONS (11 REPRESENTED IN YELLOW LINES) AND - 23.2 KJ/MOL DOCK SCORE OF COMPOUND 20, THE HIGHLY ACTIVE COMPOUND WITH ACTIVE SITE OF MRP1 PROTEIN.

The structure in the ball-and-stick model represents compound 20, and the structure in lines represents the MRP1 protein.

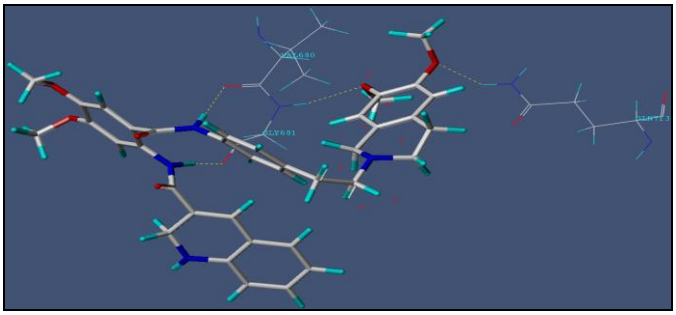

FIG.7: FIGURE SHOWING INTERACTIONS (6 REPRESENTED IN YELLOW LINES) AND -24.6 KJ/MOL DOCK SCORE OF COMPOUND 18, THE LEAST ACTIVE COMPOUND WITH ACTIVE SITE OF MRP1 PROTEIN.

The structure in ball-and-stick model represents compound 18, and the structure in lines represents MRP1 protein.

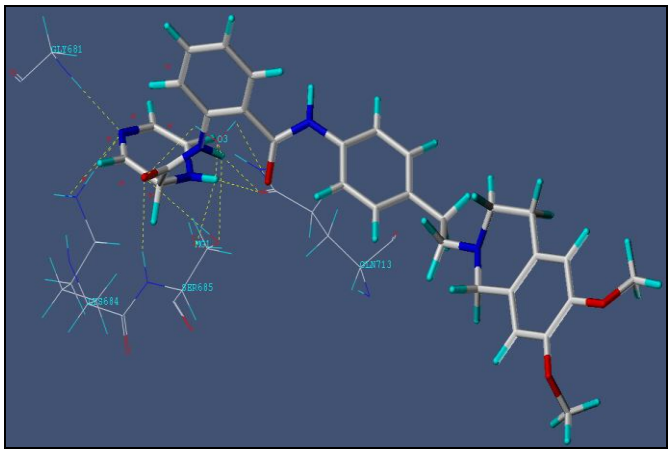

FIG. 8: COMPOUND 2 SHOWING SIX INTERACTIONS (REPRESENTED IN YELLOW LINES) WITH THE ACTIVE SITE OF MRP1 AND HAVING THE LEAST DOCK SCORE OF -14.8 KJ/MOL.

The structure in ball-and-stick model represents compound 2, and the structure in lines represents MRP1 protein.

CoMFA and CoMSIA results agree with the experimental values, signifying tariquidar analogues as MRP1 blockers:

The CoMFA method was used for deriving a 3D-QSAR model for 21 tariquidar compounds, which are reported as multi drug resistance modulators. The molecules were aligned, one over the other, to generate a common-core ring structure. Molecules that do not have a common-core ring were not included in the study. **Fig.9** shows the alignment of 26 molecules and the common-core ring. The leave-one-out partial least-squares (PLS) analysis of the obtained model yielded a high, cross-validated q^2-value of 0.698 (five components) and a non-cross-validated correlation-coefficient, r^2, of 0.983. This correlation coefficient suggests that our model is reliable and accurate.

Table 2 lists CoMFA and CoMSIA experimental activities**,** predicted activities, and residual values of the training set and test set. CoMFA and CoMSIA 3D-QSAR models were generated using tariquidar analogues reported to be MRP1 inhibitors. The chemical structures of all these molecules were provided in supplementary **Table 1** along with their IC_{50} and pIC_{50} activity values in supplementary table 2. Upon analyzing IC_{50} and pIC_{50} values, compound 18 was the least active compound, and compounds 20 and 26 were the most active compounds (**Table 3**).

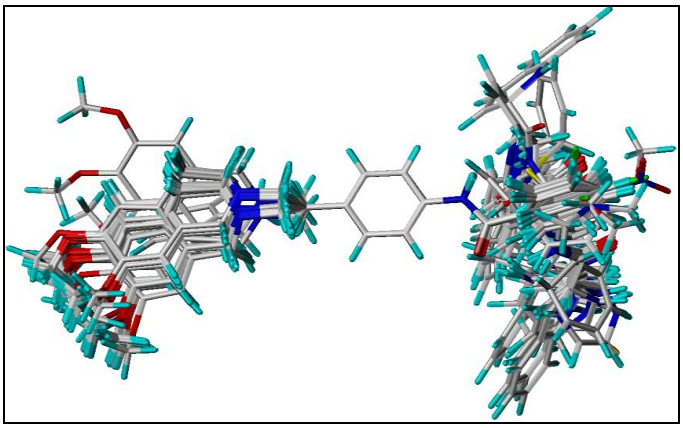

FIG. 9: THE ALIGNMENT.

The picture shows the aligned structure of all 26 tariquidar analogues and the common core ring present in all those molecules, thus aiding QSAR studies.

TABLE 2: CoMFA AND CoMSIA PREDICTED AND RESIDUAL VALUES FOR THE DATA SET.

S. No.	pIC50	COMFA		COMSIA	
		Predicted	Residual	Predicted	Residual
1	5.769551	5.921	-0.151	5.925	-0.155
2	5.568636	5.654	-0.084	5.675	-0.105
3	5.638272	5.584	0.056	5.551	0.089
4	6.00	5.28	0.72	5.94	0.06
5	6.60206	6.262	0.358	6.185	0.435
6	6.070581	6.355	-0.285	6.114	-0.044
7	6.13	5.47	0.66	5.32	0.81
8	5.481486	5.881	-0.401	5.952	-0.472
9	6.036212	5.672	0.358	5.574	0.456
10	6.69	6.91	-0.22	6.78	-0.09
11	7.173925	6.690	0.480	6.985	0.185
12	6.17	6.00	0.17	6.02	0.15

13	6.055517	6.240	-0.190	6.032	0.018
14	7.17	6.90	0.27	6.23	0.94
15	7.03	6.67	0.50	6.84	0.19
16	6.102373	6.171	-0.071	6.261	-0.473
17	7.06	7.52	-0.46	7.44	-0.38
18	5.309804	6.250	-0.950	6.108	-0.808
19	7.221849	6.776	0.454	7.249	-0.029
20	7.420216	7.005	0.145	6.785	0.635
21	6.826814	6.798	0.022	6.898	-0.078
22	6.850781	6.873	-0.023	6.119	0.731
23	6.657577	6.893	-0.243	7.123	-0.473
24	6.533132	6.725	-0.195	6.892	-0.362
25	7.346787	7.035	0.305	7.289	0.051
26	7.420216	6.774	0.646	6.817	0.603

The table indicates the experimental activities**,** predicted activities, and residual values of the training set and test set used to generate the CoMFA model. Values in grey represent the test set, and the other values represent training set.

CoMFA analysis and statistical validity predict compound 20 to be the most potent and stable MRP1 modulator:

Eleven and seven out of twenty six MRP1 inhibitors total were used in training and test sets, respectively. The compounds in the test set were chosen manually to ensure that the compounds included possess a broad activity range. The steric and electrostatic field descriptors explain 54.0 % and 46.0 % of the variance, respectively **(Table 3**). Predicted values support the statistical validity of the developed models and correlate with the experimental values, supporting the reliability of predicted CoMFA model (**Table 3**).

TABLE 3: PLS STATISTICS OF CoMFA AND CoMSIA, 3D-QSAR MODELS.

Fields	Comfa	Comsia
q^2	0.698	0.695
r^2	0.983	0.968
SEE	0.107	0.154
F	151.768	60.628
Field contribution		
Steric	54.0%	12.8%
Electrostatic	46.0%	22.7%
Hydroscopic	-	26.2%
Donor	-	0.07%
Acceptor	-	31.1%

The q^2- LOO-cross-validated correlation coefficient, r^2, non-cross-validated correlation coefficient, n- number of components used in the PLS analysis, SEE-standard error estimation, F-statistic for the analysis values shown demonstrate the accuracy and stability of our model.

CoMSIA analysis demonstrates the accuracy of predicted models:

Four major field descriptors: steric, electrostatic, hydrophobic, and hydrogen bond donor fields were used to run the CoMSIA analysis. The CoMSIA analysis demonstrated a cross-validated q^2 of 0.695, a conventional r^2 of 0.968 with a SEE of 0.154, and F value of 60.628 for training set (**Table 3**). The steric, the electrostatic, hydrophobic field, hydrogen bond donor, and hydrogen bond acceptor field descriptors explain 12.8 %, 22.7 %, 26.2 %, 0.07 % and, 31.1 % of the variance, respectively (**Table 3**). The above results demonstrate that the predicted CoMSIA model is reliable and accurate. These results demonstrate that the CoMFA and CoMSIA models can be reliably used in the design of novel MRP1 inhibitors.

Contour analysis with all the major field descriptors analyzed predict compound 20 to be the most active and stable MRP1 blocker, whereas compound 18 to be the least active and less stable one:

Contour map analysis was performed on SYBYL 6.0 to visualize the generated CoMFA and CoMSIA models. During contour map analysis, contour with contribution values of 80% for favored region and 20% for disfavored region were set as the default level.

CoMFA contour maps with steric and electrostatic contours indicate the stability of compound 20 as MRP1 blocker:

Images of CoMFA steric and electrostatic contours with lowest (compound 18) and highest activity

(compound 20) compounds are shown in **Fig's. 10** to **13**. In **Fig.10** and **11** of CoMFA – steric interactions in counter maps of tariquidar MDR modulators with lowest (compound 18) and highest activity (compound 20) – the green and yellow polyhedrons indicate regions where increased or decreased steric bulk, respectively, are predicted to enhance activity.

In the CoMFA steric contour map of compound 18, a large green contour indicating increased steric bulk was located away from the MRP1 protein whereas in the CoMFA steric contour map of compound 20, this steric bulk was found making interaction with the protein because of the additional functional groups attached (**Fig. 10** and **11**). The CoMFA electrostatic counter map of tariquidar MDR modulators with lowest (compound 18) and highest activity (compound 20) are shown in **Fig.12** and **13**. The red and blue polyhedrons indicate regions of higher electron density with high binding affinity (negative charge) and lower electron density with less affinity of the compounds to bind the protein (partial positive charge), respectively, predicting activity enhancement.

In CoMFA electrostatic contour map, a block in red representing a high electron dense region was located away from the protein whereas in CoMFA electrostatic contour map of compound 20, this highly electron-dense region was found close to the protein MRP1 (**Fig. 12** and **13**). This is possibly a reason why compound18 is less potent as a modulator and compound 20, with additional functional groups attached, is more potent. Thus, these CoMFA models demonstrate that the functional groups attached to the modulator increase its activity, thereby making it more potent.

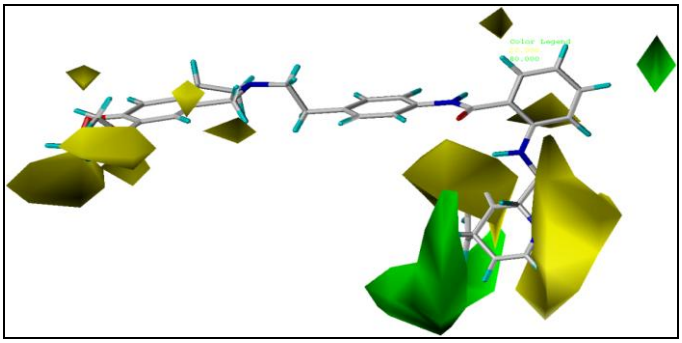

FIG.10: COMFA STERIC COUNTER MAP OF TARIQUIDAR MDR MODULATORS WITH HIGHEST ACTIVITY (COMPOUND 20).

The green and yellow polyhedrons indicate regions where increased or decreased steric bulk, respectively, are predicted to enhance activity.

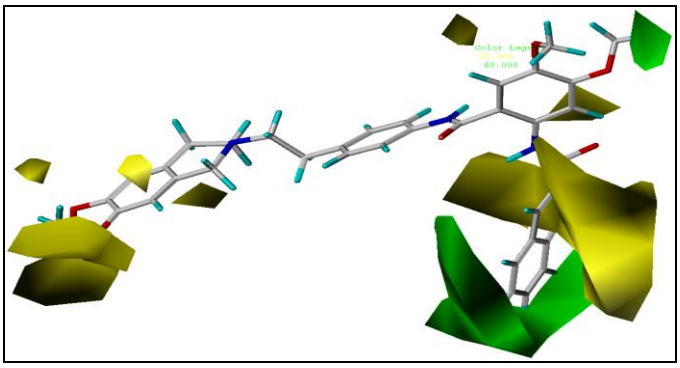

FIG.11: COMFA STERIC COUNTER MAP OF TARIQUIDAR MDR MODULATOR COMPOUND WITH LEAST ACTIVITY (COMPOUND 18).

The green and yellow polyhedrons indicate regions where increased or decreased steric bulk, respectively, are predicted to enhance activity.

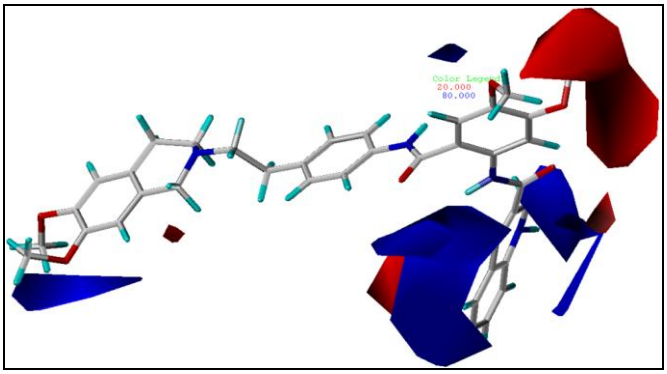

FIG. 12: COMFA ELECTROSTATIC COUNTER MAP OF TARIQUIDAR MDR MODULATORS WITH MOST ACTIVITY (COMPOUND 20).

The red and blue polyhedrons indicate regions where higher electron density (negative charge) and lower electron density (partial positive charge), respectively, are predicted to enhance activity.

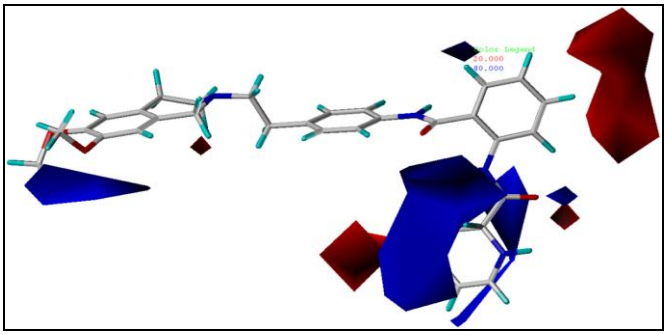

FIG.13: COMFA ELECTROSTATIC COUNTER MAP OF TARIQUIDAR MDR MODULATOR COMPOUND WITH LOWEST ACTIVITY (COMPOUND 18).

The red and blue polyhedrons indicate regions where higher electron density (negative charge) and lower electron density (partial positive charge), respectively, are predicted to enhance activity.

CoMSIA contour maps CoMFA contour maps with steric, electrostatic, hydrophobic, and hydrogen bond donor and acceptor fields indicate compound 20 to be the most active and stable MRP1 blocker:

The steric, electrostatic, hydrophobic, and hydrogen bond donor and acceptor fields were used to construct the CoMSIA contours maps (**Fig.14-23**). The steric and electrostatic contour maps of CoMFA and CoMSIA are almost identical, indicating a similar role. The CoMSIA steric and electrostatic contours maps are shown in **Fig.14** (highest activity), 15 (least activity), 16 (highest activity), and 17 (least activity), respectively. In **Fig. 15** (showing CoMSIA steric contour map of the least active compound, compound 18) steric bulk was found masking functional groups whereas in **Fig. 14**(showing CoMSIA steric contour map of modulator with highest activity, compound 20), decreased steric bulk close to the modified functional group is demonstrated to be the reason for increase in the activity.

In **Fig.15** (showing CoMSIA electrostatic contour map of least active compound, compound 18) electron density is high, indicating least activity. Electron density is low in **Fig.16** (CoMSIA electrostatic contour map of modulator with highest activity, compound 20) demonstrating that the decreased electron density enhances the activity of the molecule.

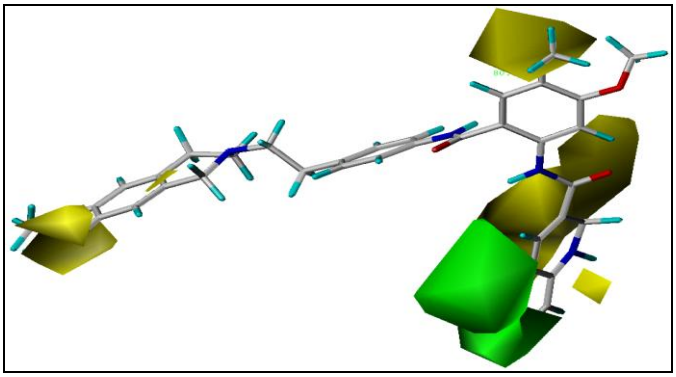

FIG. 14: COMSIA STERIC COUNTER MAPS OF TARIQUIDAR MDR MODULATORS HAVING HIGHEST ACTIVITY (COMPOUND 20).

The green and yellow polyhedrons indicate regions where increased or decreased steric bulk, respectively, are predicted to enhance activity.

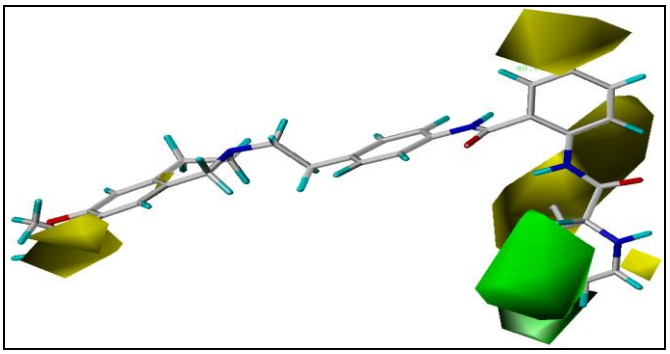

FIG. 15: COMSIA STERIC COUNTER MAPS OF TARIQUIDAR MDR MODULATORS HAVING LOWEST ACTIVITY (COMPOUND 18).

The green and yellow polyhedrons indicate regions where increased or decreased steric bulk, respectively, are predicted to enhance activity.

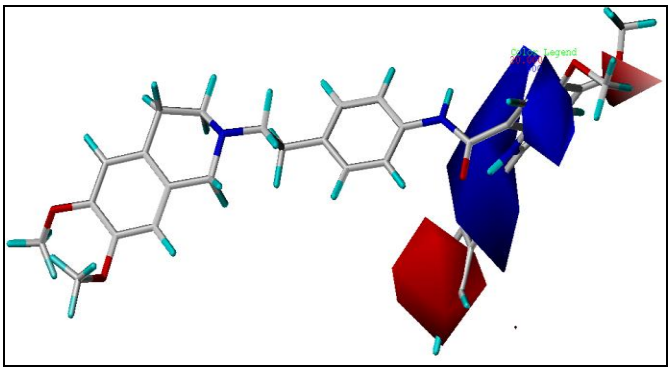

FIG.16: COMSIA ELECTROSTATIC COUNTER MAPS OF TARIQUIDAR MDR MODULATORS HAVING HIGHEST ACTIVITY (COMPOUND 20).

The red and blue polyhedrons indicate regions where higher electron density (negative charge) and lower electron density (partial positive charge), respectively, are predicted to enhance activity.

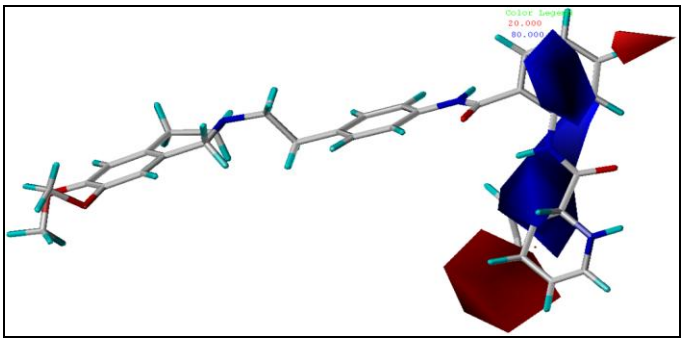

FIG. 17: COMSIA ELECTROSTATIC COUNTER MAPS OF TARIQUIDAR MDR MODULATORS HAVING LOWEST ACTIVITY (COMPOUND 18).

The red and blue polyhedrons indicate regions where higher electron density (negative charge) and lower electron density (partial positive charge), respectively, are predicted to enhance activity. The CoMSIA hydrophobic counter maps of tariquidar MDR modulators having lowest (compound 18) and highest activity (compound 20) are shown in **Fig.19** and **18**. The favourable hydrophobic region is represented by white contours, and unfavourable regions are represented by yellow contours. In **Fig. 19**, CoMSIA hydrophobic contour map of compound 18, yellow contours representing unfavourable regions are seen, indicating the least activity of molecule.

In **Fig.18**, CoMSIA hydrophobic contour map of compound 20, hydrophobicity is found masking the functional groups thereby making the molecule more potent. This indicates that the hydrophobicity will favour the binding of modulator with MRP1 thereby enhancing the activity of compound 20 and hindering the binding of compound 18 to MRP1.

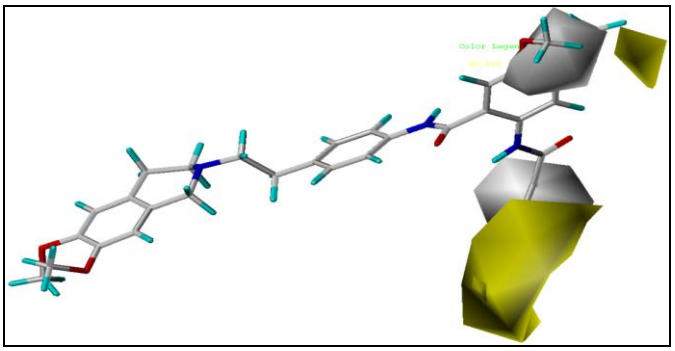

FIG. 18: COMSIA HYDROPHOBIC COUNTER MAPS OF TARIQUIDAR MDR MODULATORS HAVING HIGHEST ACTIVITY (COMPOUND 20).

The favorable hydrophobic region is represented by white contours and unfavorable regions are represented by yellow contours.

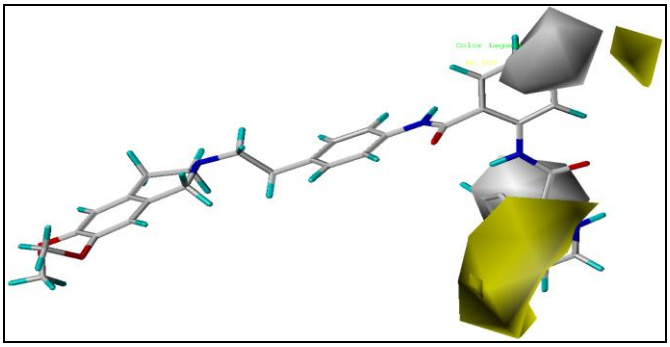

FIG. 19: COMSIA HYDROPHOBIC COUNTER MAPS OF TARIQUIDAR MDR MODULATORS HAVING LOWEST ACTIVITY (COMPOUND 18).

The favourable hydrophobic region is represented by white contours and unfavourable regions are represented by yellow contours. The CoMSIA hydrogen bond donor counter maps of tariquidar MDR modulators having lowest (compound 18) and highest activity (compound 20) are shown in **Fig. 21** and **20**. Cyan polyhedron indicates a hydrogen bond donor group in the ligand that favors biological activity, and purple polyhedrons represent hydrogen bond acceptors in the ligand that are unfavorable for bio-activity (**Fig. 20** and **21**). In the CoMSIA hydrogen bond donor counter map of compound 20, the hydrogen bond donor in cyan is present close to the functional group, and the hydrogen bond acceptor in blue that is not favorable for the activity is present away from the functional group (**Fig. 20**). This indicates that the activity of molecule 20 is enhanced by the presence of a hydrogen bond donor that favors binding of the modulator to MRP1.

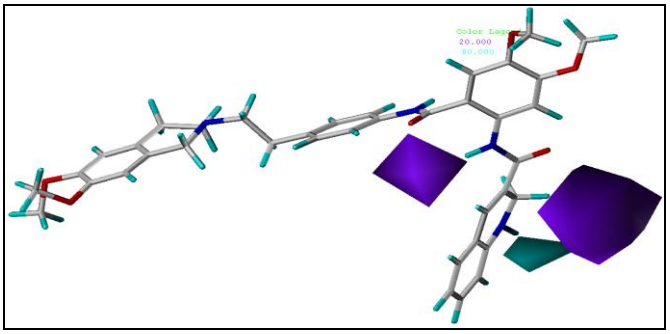

FIG. 20: COMSIA HYDROGEN DONOR OF (HYDROGEN BOND) COUNTER MAPS OF TARIQUIDAR MDR MODULATORS HAVING HIGHEST ACTIVITY (COMPOUND 20).

Cyan polyhedron beyond the ligands where a hydrogen bond donor group in the ligand will be favorable for biological activity, and the purple polyhedron represents hydrogen bond acceptor in the ligands unfavorable for bioactivity.

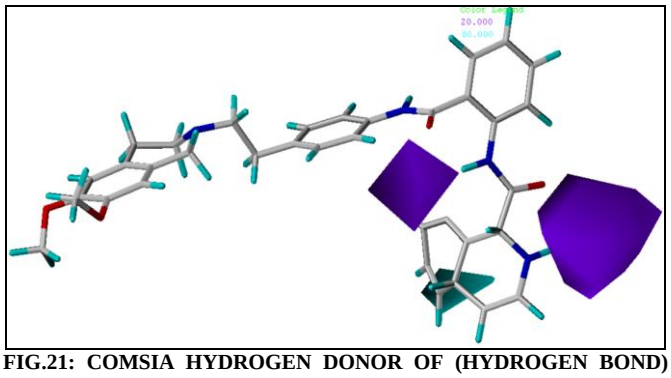

FIG.21: COMSIA HYDROGEN DONOR OF (HYDROGEN BOND) COUNTER MAPS OF TARIQUIDAR MDR MODULATORS HAVING LEAST ACTIVITY (COMPOUND 18).

Cyan polyhedron beyond the ligands where a hydrogen bond donor group in the ligand will be favorable for biological activity, and the purple polyhedron represents hydrogen bond acceptor in the ligands unfavorable for bioactivity. The CoMSIA active hydrogen bond acceptor counter maps of tariquidar MDR modulators showing lowest (compound 18) and highest activity (compound 20) are shown in **Fig. 23** and **22**. Red polyhedrons indicate a hydrogen bond donor group in the ligand that will be favorable for biological activity, and purple polyhedrons represent a hydrogen bond acceptor in the ligand that is unfavorable for bioactivity (**Fig.22** and **23**). In **Fig.22**, the purple polyhedron representing a hydrogen bond acceptor is found interacting with the functional group of compound 20 unlike that in **Fig.23** for compound 18. This suggests that the hydrogen bond acceptor and donor presence close to the functional group will determine the activity of the compound.

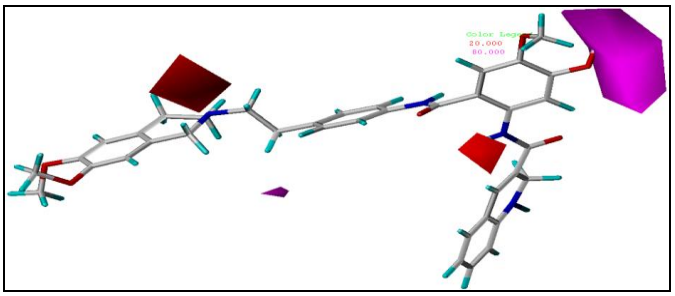

FIG. 22: COMSIA ACTIVE HYDROGEN ACCEPTOR OF (HYDROGEN BOND) COUNTER MAPS OF TARIQUIDAR MDR MODULATORS HAVING HIGHEST ACTIVITY (COMPOUND 20).

Red polyhedron beyond the ligands where a hydrogen bond donor group in the ligand will be favorable for biological activity, and the purple polyhedron represents hydrogen bond acceptor in the ligands unfavorable for bioactivity.

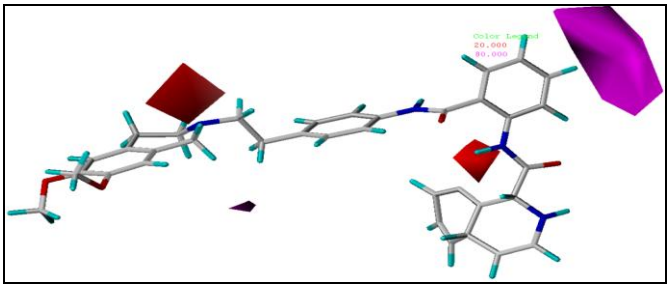

FIG.23: COMSIA ACTIVE HYDROGEN ACCEPTOR OF (HYDROGEN BOND) COUNTER MAPS OF TARIQUIDAR MDR MODULATORS HAVING LEAST ACTIVITY (COMPOUND 18).

Red polyhedron beyond the ligands where a hydrogen bond donor group in the ligand will be favorable for biological activity, and the purple polyhedron represents hydrogen bond acceptor in the ligands unfavorable for bioactivity.

DISCUSSION AND CONCLUSIONS:

In silico analysis and 3D-QSAR studies on efflux blockers are important tools in the fight against drug resistance in anti-cancer treatment [21]. Contour map analysis and docking studies on MRP1 inhibitors are critical as the MRP1 efflux pump is a major factor behind the failure of anti-cancer drug therapies [8]. The tariquidar analogues tested as MRP1 efflux inhibitors in the current study demonstrate the mechanism of inhibitor interacting with the active site of MRP1, binding it tightly; thus making the cell unable to pump anti-cancer drugs out using the blocked MRP1 efflux pumps. A receptor-independent 3D-QSAR has been established for tariquidar analogues employing the most widely used techniques CoMFA and CoMSIA. This work highlights the importance of ligand orientation and selection of the training set molecules in the development of statistically significant QSAR models.

Interestingly, the CoMSIA models provided better statistical models than CoMFA, which points to the significance of hydrogen bond donor and hydrophobic fields in the selectivity and activity of these ligands in addition to steric and electrostatic fields. The statistical significance and robustness of the generated 3D-QSAR models were confirmed using an external set of molecules. The structural requirements identified in the present study can be utilized strategically in the design of novel, potent, and unique tariquidar analogue compounds with multidrug resistance modulation activities [62].

Even though the dock score of compound 20 is not the highest (the highest dock score was compound 9 with -31.4 KJ/mol) among all the 26 compounds tested in the study, from the FlexX docking interactions and contour map analysis it can be predicted that the amino acid interactions and force fields of compound 20 with MRP1 are critical for rendering this compound potent [16]. Based on the interactions of compound 20 with the active site of MRP1 and force-field interactions we predict that

compound 20 can be effectively used in biological systems as a MRP1 inhibitor as it will be potent and stable. Compound 18, being the least active compound, has shown a FlexX dock score of -24.6 KJ/mol with six interactions. Even though the dock score of compound 18 is considerably high, it can be predicted that this compound is not stable (based on contour map analysis) and that the interactions with the active site of MRP1 (six interactions) are not strong enough to block the pump.

Therefore, from molecular simulated docking studies and from contour map analysis together, we predict that compound 20 can be demonstrated as an effective MRP1 efflux pump blocker because of its stability in the biological environment and its potency to interact with and block MRP1 pump. Quantitative structure activity relationship study (3D-QSAR) results indicate a better fit between MRP1 and the tariquidar efflux modulator analogues. The CoMFA and CoMSIA studies, PLS statistical analysis, and contour map analysis support the accuracy of predicted and docked models. From our docking simulation and contour map analysis, we predicted which tariquidar compounds out of 26 different analogues might be most effective as MRP1 efflux inhibitors. We believe that by using the methodology of this study and the predictive models therein as a base, other potential efflux pump inhibitors might be discovered. Additionally, we expect that future investigations into the tariquidar analogues identified in this study will yield innovate and effective MRP1 blockers, thereby enhancing the efficacy of anti-cancer therapy.

ACKNOWLEDGEMENTS: This work was made possible by the NM-INBRE program grant P20GM103451 from the National Center for Research Resources. This publication was also supported by an internal research grant awarded by the Department of Biology, Eastern New Mexico University, Portales, New Mexico, USA.

AUTHORS' CONTRIBUTIONS:

Authors' contributions	PK	MI	TMW	RK	US	ARD	SKG	IR	SB	AH	MFV
Research concept and design	✓	--	--	--	--	--	--	--	--	--	✓
Figures and tables	✓	✓	--	✓	✓	✓	✓	--	--	--	✓
Collection and/or assembly of data	✓	✓	--	--	--	--	✓	--	--	--	--
Data analysis and interpretation	✓	✓	--	--	--	✓	✓	--	--	--	--
Writing the article	✓	✓	--	--	--	✓	--	--	--	--	--
References	✓	--	--	--	--	--	--	--	--	--	✓
Revision of the article	✓	✓	✓	✓	✓	✓	✓	✓	✓	✓	✓
Critical revision of article	--	--	--	--	--	--	--	--	--	--	✓
Final approval of article	✓	✓	✓	✓	✓	✓	✓	✓	✓	✓	✓
Statistical analysis	✓	✓	--	--	--	✓	✓	--	--	--	--

REFERENCES:

1. Sun, Y., et al., Role of ABC transporters in cancer chemotherapy. Chin J Cancer, 2012. 31(2): p. 51-7.
2. SYBYL-X 1.2, Tripos International, 1699 South Hanley Rd., St. Louis, Missouri, 63144, USA.
3. Rexer, B.N. and C.L. Arteaga, Intrinsic and Acquired Resistance to HER2-Targeted Therapies in HER2 Gene-Amplified Breast Cancer: Mechanisms and Clinical Implications. Critical Reviews in Oncogenesis, 2012. 17(1): p. 1-16.
4. Xu, F., et al., Differential drug resistance acquisition to doxorubicin and paclitaxel in breast cancer cells. Cancer Cell Int, 2014. 14(1): p. 538.
5. Kumar, S. and M.F. Varela, Biochemistry of Bacterial Multidrug Efflux Pumps. International Journal of Molecular Sciences, 2012. 13(4): p. 4484-4495.
6. Vinogradov, S. and X. Wei, Cancer stem cells and drug resistance: the potential of nanomedicine. Nanomedicine (London, England), 2012. 7(4): p. 597-615.
7. Moitra, K., H. Lou, and M. Dean, Multidrug efflux pumps and cancer stem cells: insights into multidrug resistance and therapeutic development. Clin Pharmacol Ther, 2011. 89(4): p. 491-502.
8. Pajeva, I.K. and M. Wiese, Structure–Activity Relationships of Tariquidar Analogs as Multidrug Resistance Modulators. The AAPS Journal, 2009. 11(3): p. 435-444.
9. Karol M Pawłowski, Joanna Mucha, Kinga Majchrzak, Tomasz Motyl and Magdalena Król, Expression and role of PGP, BCRP, MRP1 and MRP3 in multidrug resistance of canine mammary cancer cells.BMC Veterinary research, 2013. 9(119): p. 1-10.
10. Deng J1, Shao J, Markowitz JS, An G., ABC transporters in multi-drug resistance and ADME-Tox of small molecule tyrosine kinase inhibitors.Pharmaceutical research, 2014. 31(9): p. 2237-55.
11. Ramaen, O., et al., Structure of the Human Multidrug Resistance Protein 1 Nucleotide Binding Domain 1 bound

to Mg2+/ATP Reveals a Non-productive Catalytic Site. J Mol Biol, 2006. 359(4): p. 940-949.
12. Popęda M 1, Płuciennik E 2, Bednarek AK ., Proteins in cancer multidrug resistance .Postępy higieny i medycyny doświadczalnej (Online), 2014. 20(68): p. 616-32.
13. Chang, X.B., Molecular mechanism of ATP-dependent solute transport by multidrug resistance-associated protein 1. Methods Mol Biol, 2010. 596: p. 223-49.
14. He SM1, Li R, Kanwar JR, Zhou SF., Structural and functional properties of human multidrug resistance protein 1 (MRP1/ABCC1).Current medicinal Chem, 2011. 18(3): p. 439-81.
15. Kohan HG1, Boroujerdi M.., Time and concentration dependency of P-gp, MRP1 and MRP5 induction in response to gemcitabine uptake in Capan-2 pancreatic cancer cells. Xenobiotica, 2015. 45(17): p. 1757-68.
16. Chang XB., Molecular mechanism of ATP-dependent solute transport by multidrug resistance-associated protein 1.Cancer metastatis Rev, 2007. 26(1): p. 15-37.
17. Kunická T1, Souček P., Importance of ABCC1 for cancer therapy and prognosis. Drug Metab Rev, 2014.46(3):p. 325-42.
18. He, S.M., et al., Structural and functional properties of human multidrug resistance protein 1 (MRP1/ABCC1). Curr Med Chem, 2011. 18(3): p. 439-81.
19. Wind, N.S. and I. Holen, Multidrug Resistance in Breast Cancer: From In Vitro Models to Clinical Studies. International Journal of Breast Cancer, 2011. 2011.
20. Molnár J1, Engi H, Hohmann J, Molnár P, Deli J, Wesolowska O, Michalak K, Wang Q., Reversal of multidrug resitance by natural substances from plants.Curr Top Med Chem, 2010. 10(47): p. 7512-23.
21. Surtaj H. Iram and Susan P. C. Cole., Expression and Function of Human MRP1 (ABCC1) Is Dependent on Amino Acids in Cytoplasmic Loop 5 and Its Interface with Nucleotide Binding Domain 2.J Biol Chem, 2011. 286: p. 7202-7213.
22. Chang, X.B., A molecular understanding of ATP-dependent solute transport by multidrug resistance-associated protein MRP1. Cancer Metastasis Rev, 2007. 26(1): p. 15-37.
23. Huang L, Perrault C, Coelho-Martins J, Hu C, Dulong C, Varna M, Liu J, Jin J, Soria C, Cazin L, Janin A, Li H, Varin R, Lu H., Induction of acquired drug resistance in endothelial cells and its involvement in anticancer therapy.H Hematol Oncol, 2013. 9(6): p. 6-49.
24. Qosa H1, Miller DS2, Pasinelli P3, Trotti D., Regulation of ABC efflux transporters at blood-brain barrier in health and neurological disorders. Brain Res, 2015. S0006-8993(15):p. 00530-2.
25. Montanari F1, Ecker GF., ABC Prediction of drug-ABC-transporter interaction--Recent advances and future challenges.Adv Drug Deliv Rev, 2015. 23(86): p. 117-26.
26. Robey, R.W., et al., Rapid detection of ABC transporter interaction: Potential utility in pharmacology. Journal of Pharmacological and Toxicological Methods, 2011. 63(3): p. 217-222.
27. Fox, E. and S.E. Bates, Tariquidar (XR9576): a P-glycoprotein drug efflux pump inhibitor. Expert Rev Anticancer Ther, 2007. 7(4): p. 447-59.
28. Egger, M., et al., Tariquidar Analogues: Synthesis by CuI-Catalysed N/O–Aryl Coupling and Inhibitory Activity against the ABCB1 Transporter. European Journal of Organic Chemistry, 2007. 2007(16): p. 2643-2649.
29. Varela, M.F., S. Kumar, and G. He, Potential for inhibition of bacterial efflux pumps in multidrug-resistant Vibrio cholera. The Indian Journal of Medical Research, 2013. 138(3): p. 285-287.
30. Kumar, S., M.M. Mukherjee, and M.F. Varela, Modulation of Bacterial Multidrug Resistance Efflux Pumps of the Major Facilitator Superfamily. International Journal of Bacteriology, 2013: p. 15.
31. Abdallah HM, Al-Abd AM, El-Dine RS, El-Halawany AM., P-glycoprotein inhibitors of natural origin as potential tumor chemo-sensitizers: A review.J Adv Res, 2015. 6(1): p. 45-62.
32. Bansal T, Jaggi M, Khar RK, Talegaonkar S, Emerging significance of flavonoids as P-glycoprotein inhibitors in cancer chemotherapy. J Pharm Pharm Sci, 2010. 12(1): p. 46-78.
33. Kuhnle, M., et al., Potent and selective inhibitors of breast cancer resistance protein (ABCG2) derived from the p-glycoprotein (ABCB1) modulator tariquidar. J Med Chem, 2009. 52(4): p. 1190-7.
34. Wiese M, BCRP/ABCG2 inhibitors: a patent review (2009 - present).Expert Opin Ther Pat. 2015. 10:p. 1-9.
35. Coley HM, Overcoming multidrug resistance in cancer: clinical studies of p-glycoprotein inhibitors.Methods Mol Biol, 2010. 596:P. 341-58.
36. Li XQ, Wang L, Lei Y, Hu T, Zhang FL, Cho CH, To KK, Reversal of P-gp and BCRP-mediated MDR by tariquidar derivatives.Eur J Med Chem, 2015. 28(101):P. 560-72.
37. Kakarla, P., et al., Molecular modelling, 3D-QSAR, and drug docking studies on the role of natural anticoagulant compounds in antithrombotic therapy. International Journal of Pharmaceutical Sciences and Research, 2014. 5(10): p. 4141-4152.
38. Mishra RK1, Singh J, A Structure Guided QSAR: A Rapid and Accurate technique to predict IC50: A Case Study.Curr Comput Aided Drug Des, 2015. 11(2):p. 152-63.
39. Cross, S.S., Improved FlexX docking using FlexS-determined base fragment placement. J Chem Inf Model, 2005. 45(4): p. 993-1001.
40. Verma J1, Khedkar VM, Coutinho EC, 3D-QSAR in drug design--a review.Curr Top Med Chem, 2010. 10(1): p. 95-115.
41. Tsai, K.C., et al., A comparison of different electrostatic potentials on prediction accuracy in CoMFA and CoMSIA studies. Eur J Med Chem, 2010. 45(4): p. 1544-51.
42. Cho, S.J. and A. Tropsha, Cross-validated R2-guided region selection for comparative molecular field analysis: a simple method to achieve consistent results. J Med Chem, 1995. 38(7): p. 1060-6.
43. Lam, K.P., Contour map registration using fourier descriptors of gradient codes. IEEE Trans Pattern Anal Mach Intell, 1985. 7(3): p. 332-8.
44. Ishikawa T1, Saito H, Hirano H, Inoue Y, Ikegami Y, Human ABC transporter ABCG2 in cancer chemotherapy: drug molecular design to circumvent multidrug resistance.Methods Mol Biol, 2012. 910:p. 267-78.
45. Qiao LS, He YS, Zhang YL, Study on structure-activity relationship of flavonoids' multidrug resistance-associated protein inhibitory activity.Zhongguo Zhong Yao Za Zhi, 2014. 39(5):p. 885-90.
46. Wang T, Wu MB, Lin JP, Yang LR, Quantitative structure-activity relationship: promising advances in drug discovery platforms. Expert Opin Drug Discov, 2015. 11:p. 1-18.
47. Sedykh A, Fourches D, Duan J, Hucke O, Garneau M, Zhu H, Bonneau P, Tropsha A., Human intestinal transporter database: QSAR modeling and virtual profiling of drug

48. uptake, efflux and interactions.Pharm Res, 2013. 30(4):p. 996-1007.
49. Kumar SP1, Jha PC, Jasrai YT, Pandya HA, The effect of various atomic partial charge schemes to elucidate consensus activity-correlating molecular regions: a test case of diverse QSAR models.J Biomol Struct Dyn, 2015. 21:p. 1-20.
50. Gasteiger, J. and M. Marsili, Iterative partial equalization of orbital electronegativity—a rapid access to atomic charges. Tetrahedron, 1980. 36(22): p. 3219-3228.
51. Stewart, J.J., MOPAC: a semiempirical molecular orbital program. J Comput Aided Mol Des, 1990. 4(1): p. 1-105.
52. Maltarollo VG1, Gertrudes JC, Oliveira PR, Honorio KM, Applying machine learning techniques for ADME-Tox prediction: a review. Expert Opin Drug Metab Toxicol, 2015. 11(2):p. 259-71.
53. Bohm, M. and G. Klebe, Development of new hydrogen-bond descriptors and their application to comparative molecular field analyses. J Med Chem, 2002. 45(8): p. 1585-97.
54. Liu, F.F., et al., Rational design of affinity peptide ligand by flexible docking simulation. J Chromatogr A, 2007. 1146(1): p. 41-50.
55. Seethalakshmi Sreenivasan1, Sathyabaarathi Ravichandran2, Umashankar Vetrivel2, Subramanian Krishnakumar, Modulation of multidrug resistance 1 expression and function in retinoblastoma cells by curcumin.J of Pharm and Pharmacotherapeutics, 2013. 2(4): p. 103-109.
56. Bello, M., M. Martinez-Archundia, and J. Correa-Basurto, Automated docking for novel drug discovery. Expert Opin Drug Discov, 2013. 8(7): p. 821-34.
57. Srivastava, V., et al., CoMFA and CoMSIA 3D-QSAR analysis of DMDP derivatives as anti-cancer agents. Bioinformation, 2012. 2(9): p. 384-391.
58. Marcoline FV, Bethel N, Guerriero CJ, Brodsky JL, Grabe M, Membrane Protein Properties Revealed through Data-Rich Electrostatics Calculations.Structure, 2015. 23(8):p. 1526-37.
59. Rao F, Protein inherent structures by different minimization strategies.J Comput Chem, 2011. 32(6):p. 1113-6.
60. Melville, J.L. and J.D. Hirst, On the stability of CoMFA models. J Chem Inf Comput Sci, 2004. 44(4): p. 1294-300.
61. Stanton DT, QSAR and QSPR model interpretation using partial least squares (PLS) analysis.Curr Comput Aided Drug Des, 2012. 8(2):p. 107-27.
62. Brooks BR, Brooks CL, Mackerell AD, Nilsson L, Petrella RJ, Roux B, Won Y, Archontis G, Bartels C, Boresch S, Caflisch A, Caves L, Cui Q, Dinner AR, Feig M, Fischer S, Gao J, Hodoscek M, Im W, Kuczera K, Lazaridis T, Ma J, Ovchinnikov V, Paci E, Pastor RW, Post CB, Pu JZ, Schaefer M, Tidor B, Venable RM, Woodcock HL, Wu X, Yang W, York DM, Karplus M, CHARMM: the biomolecular simulation program.J Comput Chem, 2009. 30(10):p. 1545-614.

How to cite this article:
Kakarla P, Inupakutika M, Devireddy AR, Gunda SK, Willmon TM, Ranjana KC, Shrestha U, Ranaweera I, Hernandez AJ and Varela MF: 3d-QSAR and Contour Map Analysis of Tariquidaranalogues as Multidrug Resistanceprotein-1 (Mrp1) Inhibitors. Int J Pharm Sci Res 2016; 7(2): 554-72.doi: 10.13040/IJPSR.0975-8232.7(2).554-72.